The Astrophysical Journal Letters, 937:L12 (11pp), 2022 September 20 https://doi.org/10.3847/2041-8213/ac90ba


# Cooling Envelope Model for Tidal Disruption Events

Brian D. Metzger[1,2]
[1] Department of Physics and Columbia Astrophysics Laboratory, Columbia University, New York, NY 10027, USA; bmetzger@phys.columbia.edu
[2] Center for Computational Astrophysics, Flatiron Institute, 162 5th Ave., New York, NY 10010, USA
*Received 2022 July 21; revised 2022 August 25; accepted 2022 September 9; published 2022 September 21*

## Abstract

We present a toy model for the thermal optical/UV/X-ray emission from tidal disruption events (TDEs). Motivated by recent hydrodynamical simulations, we assume that the debris streams promptly and rapidly circularize (on the orbital period of the most tightly bound debris), generating a hot quasi-spherical pressure-supported envelope of radius $R_v \sim 10^{14}$ cm (photosphere radius $\sim 10^{15}$ cm) surrounding the supermassive black hole (SMBH). As the envelope cools radiatively, it undergoes Kelvin–Helmholtz contraction $R_v \propto t^{-1}$, its temperature rising $T_{\rm eff} \propto t^{1/2}$ while its total luminosity remains roughly constant; the optical luminosity decays as $\nu L_\nu \propto R_v^2 T_{\rm eff} \propto t^{-3/2}$. Despite this similarity to the mass fallback rate $\dot{M}_{\rm fb} \propto t^{-5/3}$, envelope heating from fallback accretion is subdominant compared to the envelope cooling luminosity except near optical peak (where they are comparable). Envelope contraction can be delayed by energy injection from accretion from the inner envelope onto the SMBH in a regulated manner, leading to a late-time flattening of the optical/X-ray light curves, similar to those observed in some TDEs. Eventually, as the envelope contracts to near the circularization radius, the SMBH accretion rate rises to its maximum, in tandem with the decreasing optical luminosity. This cooling-induced (rather than circularization-induced) delay of up to several hundred days may account for the delayed onset of thermal X-rays, late-time radio flares, and high-energy neutrino generation, observed in some TDEs. We compare the model predictions to recent TDE light-curve correlation studies, finding both agreement and points of tension.

*Unified Astronomy Thesaurus concepts:* Tidal disruption (1696); Accretion (14)

## 1. Introduction

A tidal disruption event (TDE) occurs when a star orbiting a supermassive black hole (SMBH) on what is typically a parabolic orbit comes sufficiently close to the SMBH to be strongly compressed and torn apart by tidal forces (Hills 1975; Rees 1988; Evans & Kochanek 1989; Guillochon & Ramirez-Ruiz 2013; Stone et al. 2013; Coughlin & Nixon 2022).

When TDE flares were first discovered in UV (e.g., Stern et al. 2004; Gezari et al. 2006) and optical (e.g., van Velzen et al. 2011; Cenko et al. 2012; Arcavi et al. 2014) surveys, one largely (but not wholly; Loeb & Ulmer 1997) unexpected discovery were their high optical luminosities $L_{\rm opt} \gtrsim 10^{43}$ erg s$^{-1}$, modest effective temperatures $T_{\rm eff} \approx 10^{4.2}$–$10^{4.7}$ K, and correspondingly large photosphere radii $\approx 10^{14}$–$10^{15}$ cm (e.g., Arcavi et al. 2014; Holoien et al. 2014; Hung et al. 2017; van Velzen et al. 2021a; see Gezari 2021 for a recent review). It was previously a common assumption that once the tidal streams of the disrupted star dissipate their bulk kinetic energy ("circularize"), the resulting structure would be a compact disk orbiting the SMBH comparable in size to the tidal sphere (typically tens or hundreds of gravitational radii, or $\sim 10^{13}$ cm for $10^6$–$10^7\,M_\odot$ SMBHs), which produces multicolor blackbody emission peaking in the soft X-ray bands (e.g., Rees 1988; Cannizzo et al. 1990; Lodato & Rossi 2011) with only a tiny fraction of the luminosity radiated at optical/UV frequencies.

After reaching peak luminosity, many TDE optical light curves decay following a $\propto t^{-5/3}$ power law (e.g., Gezari et al. 2006; Hung et al. 2017), thus appearing to track the rate of mass fallback for complete disruptions (Phinney 1989; Guillochon & Ramirez-Ruiz 2013), also in conflict with the shallower decay predicted by $\alpha$-disk models (e.g., Lodato & Rossi 2011). However, in other cases the post-maximum decay is better fit as an exponential (e.g., Holoien et al. 2016; Blagorodnova et al. 2017) and/or exhibits a flattening at late times (e.g., Leloudas et al. 2016; van Velzen et al. 2019; Wevers et al. 2019). Thermal X-rays are detected from a subset of optically selected TDEs, but the X-ray rise is frequently significantly delayed, by up to hundreds of days, with respect to the optical peak (e.g., Gezari et al. 2006, 2017; Kajava et al. 2020; Liu et al. 2022; Yao et al. 2022). Late-time TDE X-ray light curves also frequently decay at a rate more shallow than $\propto t^{-5/3}$ (e.g., Holoien et al. 2016; Auchettl et al. 2017), which has been attributed to a mismatch between the SMBH accretion rate and fallback rate due to the viscous time of the disk (e.g., Cannizzo et al. 1990; Shen & Matzner 2014; Auchettl et al. 2017).

In part to address these rapidly growing observational data, numerical (magneto)hydrodynamical simulations of TDEs have been developed over the past decade (e.g., Guillochon & Ramirez-Ruiz 2013; Hayasaki et al. 2013; Shiokawa et al. 2015; Bonnerot et al. 2016b; Hayasaki et al. 2016; Sadowski et al. 2016; Steinberg et al. 2019; Bonnerot & Lu 2020; Ryu et al. 2021; Andalman et al. 2022; Steinberg & Stone 2022). Many of these efforts aim to determine what processes lead to debris circularization, with a major focus on physical collisions between outgoing and incoming bound debris streams (e.g., Hayasaki et al. 2013; Shiokawa et al. 2015; Lu & Bonnerot 2020), and how such collisions are hastened or delayed by effects such as cooling or general relativistic precession (e.g., Dai et al. 2015; Guillochon & Ramirez-Ruiz 2015; Bonnerot & Stone 2021; Andalman et al. 2022).

These issues bear crucially on the energy source powering TDE flares. If circularization is significantly delayed (e.g., by

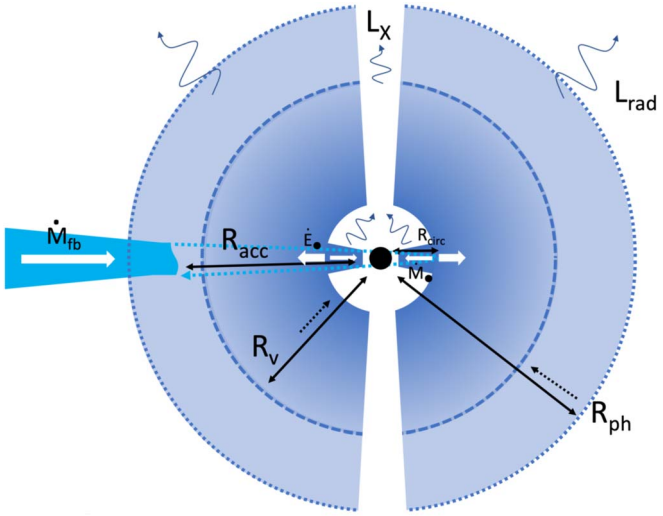


**Figure 1.** Schematic illustration of the model. Rapid circularization of the TDE debris forms a quasi-circular pressure-supported envelope around the SMBH of characteristic radius $R_v$ and photosphere radius $R_{\rm ph} \sim 10R_v$ that powers the early optical emission. The envelope luminosity $L_{\rm rad}$ primarily derives from the gravitational energy released from its cooling-driven contraction at close to the Eddington limit, though fallback accretion (which deposits its energy at a radius $R_{\rm acc} \gtrsim R_v$, where the stream dissolves inside the envelope after passing through pericenter) may contribute significantly at early times. As the envelope cools and contracts, roughly as $R_v \propto R_{\rm ph} \propto t^{-1}$ initially, the effective temperature rises $T_{\rm eff} \propto t^{1/2}$ while the optical luminosity $\nu L_\nu \propto R_{\rm ph}^2 T_{\rm eff} \propto t^{-3/2}$ drops. The SMBH accretion rate rises in tandem, as controlled by the envelope density and viscous time near the circularization radius, potentially powering thermal X-ray and/or jetted activity along the initially narrow polar funnel. The inner accretion flow also acts as a source of energy to the envelope, which can delay the envelope's contraction in a regulated manner, flattening the late-time optical and X-ray light-curve decay.

many orbits of the most tightly bound debris), then powering the optical luminosities of TDEs requires tapping directly into the limited amount of energy dissipated by stream–stream collisions (e.g., Piran et al. 2015). On the other hand, if even a modest fraction of the bound debris reaches small scales around the SMBH, the resulting accretion power can be sufficient to power the observed UV/optical emission, e.g., via the reprocessing of disk-emitted X-rays by radially extended material (e.g., Metzger & Stone 2016; Roth et al. 2016; Dai et al. 2018), such as bound tidal debris (e.g., Guillochon & Ramirez-Ruiz 2013), wide-angle unbound outflows generated during the circularization process (e.g., Metzger & Stone 2016; Lu & Bonnerot 2020), or accretion disk winds (e.g., Strubbe & Quataert 2009; Miller 2015; Dai et al. 2018; Wevers et al. 2019). The geometric beaming of thermal X-rays from the inner accretion flow along the low-density polar regions of the reprocessing structure offers a unification scheme for the optical and X-ray properties of TDEs based on the observer viewing angle (e.g., Metzger & Stone 2016; Dai et al. 2018). However, while some TDEs exhibit clear evidence for outflows (e.g., Miller et al. 2015; Alexander et al. 2017; Kara et al. 2018), the mass-loss rates required to sustain the large photosphere radii in outflow reprocessing scenarios may in some events be unphysically large (e.g., Matsumoto & Piran 2021).

Some observations hint that the peak SMBH accretion rate can be significantly delayed with respect to the optical peak. While a handful of powerful jetted TDEs exhibit bright nonthermal X-ray and radio emission (e.g., Bloom et al. 2011; Burrows et al. 2011), most TDEs are radio dim (e.g., Alexander et al. 2020), excluding powerful off-axis jets (e.g., Generozov et al. 2017). Nevertheless, several TDEs exhibit late-time radio flares, indicating mildly relativistic material ejected from the vicinity of the SMBH, but delayed from the optical peak by several months to years (e.g., Horesh et al. 2021a, 2021b; Cendes et al. 2022; Sfaradi et al. 2022). A potentially related occurrence is the coincident detection of high-energy neutrinos from three optical TDEs by IceCube (van Velzen et al. 2021b; Stein et al. 2021; Reusch et al. 2022), each of which also arrived several months after the optical peak. State transitions in the accretion flow offer one potential explanation for the delayed onset of jetted accretion activity (e.g., Giannios & Metzger 2011; Tchekhovskoy et al. 2014). Delayed circularization leading to delayed disk formation (as invoked to explain similarly delayed rises in the X-ray emission; e.g., Gezari et al. 2017) offers another.

Even rapid and efficient circularization may not, however, create a compact disk, at least initially. Loeb & Ulmer (1997) assume that the TDE debris forms a spherical radiation-dominated hydrostatic envelope encasing the SMBH. Coughlin & Begelman (2014) emphasize that the low angular momenta of TDE debris relative to their binding energy (i.e., "circularization" radii $\ll$ "virial" radii) endow the circularized structure with properties quite unlike thin Keplerian disks, due to their much larger radial extent and propensity to launch outflows/jets along an extremely narrow polar funnel. While this structure may briefly manifest as a high-eccentricity disk (e.g., Cao et al. 2018; Liu et al. 2021), dissipation within this geometrically thick (e.g., Steinberg & Stone 2022) confluence of differentially precessing annuli will likely be strong (e.g., Bonnerot et al. 2017; Ryu et al. 2021). And once thermal pressure provides the support against gravity, the bound debris may arguably be modeled most simply as a quasi-spherical "envelope" (Loeb & Ulmer 1997). A quasi-spherical emission surface is supported by spectropolarimetry observations of some TDEs (e.g., Patra et al. 2022).

Recently, Steinberg & Stone (2022) presented three-dimensional radiation hydrodynamical simulations of the tidal disruption of a solar-mass star by a $10^6\ M_\odot$ black hole, for the most common (but most computationally challenging) case of a $\beta = 1$ orbit penetration factor. Unlike the findings or assumptions of most previous works, they find rapid circularization of the debris streams within a short time ($\lesssim$70 days), comparable to the fallback time of the most tightly bound debris. A possible explanation for their result is stronger tidal compression and heating of the streams as they pass through pericenter compared to that found in previous work (e.g., Guillochon & Ramirez-Ruiz 2013; Bonnerot & Lu 2022) owing to the inclusion of recombination energy in the assumed equation of state. Steinberg & Stone (2022) further show that radiative diffusion from the extended circularized envelope generates a rising optical light curve with an effective temperature consistent with those of optically selected TDE flares. Rapid circularization was also found in general relativistic hydrodynamical simulations of a similar $1{:}10^6$ mass ratio system by Andalman et al. (2022), in the case of a higher $\beta = 7$ encounter for which rapid stream–stream collisions driven by general relativistic precession play a decisive role in circularization.

Motivated in part by these recent findings of rapid circularization even across the most commonly sampled regions of TDE parameter space, here we present a model for

the long-term evolution and emission from TDE envelopes following their formation. Though following in spirit Loeb & Ulmer (1997), we make different assumptions and track the time evolution of the envelope size in light of various cooling and heating processes, including SMBH feedback. The proposed model of TDE emission as being driven by the thermal evolution of a spherical envelope, while clearly oversimplified in many respects, may nevertheless provide a new view on open questions, such as the timescale and shape of the light-curve decay and the origin of the observed delay between the optical peak and those physical processes (soft X-ray emission, radio flares, fast outflows, neutrino production) instead driven by the innermost SMBH accretion flow.

This paper is organized as followed. In Section 2 we present the model for the envelope evolution. In Section 3 we present our results, first focusing on a single fiducial model and dissecting the impact of different physical processes (Section 3.1) and then comparing the light-curve predictions across a range of star and SMBH properties to TDE observations (Section 3.2). In Section 4 we summarize our findings, expand on some implications, and comment on directions for future work.

## 2. Model

We model the long-term evolution of a quasi-spherical TDE envelope under the assumption of prompt circularization (see Figure 1 for a schematic illustration). We first describe the initial conditions imparted by the tidal disruption process (Section 2.1) and then the details of the envelope evolution (Section 2.2).

### 2.1. Tidal Disruption and Envelope Formation

A star of mass $M_\star = m_\star M_\odot$ and radius $R_\star$ is tidally disrupted if the pericenter radius of its orbit, $R_p$, becomes less than the tidal radius (e.g., Hills 1975)

$$R_t \approx R_\star (M_\bullet/M_\star)^{1/3} \approx 7 \times 10^{12}\ \mathrm{cm}\ m_\star^{7/15} M_{\bullet,6}^{1/3} \approx 47 m_\star^{7/15} M_{\bullet,6}^{-2/3} R_g, \quad (1)$$

where $M_\bullet$ is the SMBH mass, $R_g \equiv GM_\bullet/c^2$, and we assume here and in analytic estimates to follow a mass–radius relationship $R_\star \approx m_\star^{4/5} R_\odot$ appropriate to lower main-sequence stars. The orbital penetration factor is defined as $\beta \equiv R_t/R_p > 1$.

Disruption binds roughly half the star to the SMBH by a specific energy $|E_t| = kGM_\bullet R_\star/R_t^2$ corresponding roughly to the work done by tidal forces over a distance $\sim R_t$. The most tightly bound matter falls back to the SMBH on the characteristic fallback timescale set by the period of an orbit with energy $E_t$,

$$t_{\rm fb} \simeq 58\ \mathrm{days} \left(\frac{k}{0.8}\right)^{-3/2} M_{\bullet,6}^{1/2} m_\star^{1/5}, \quad (2)$$

where the factor $k$ has a weak dependence on the penetration factor $\beta$ (Stone et al. 2013; Guillochon & Ramirez-Ruiz 2013) and hereafter we shall take $k \simeq 0.8$ corresponding to a $\beta = 1$ disruption for a $\gamma = 5/3$ polytropic star. The resulting rate of mass fallback at time $t \gg t_{\rm fb}$ is given by

$$\dot{M}_{\rm fb} \approx \frac{2M_{\rm acc}}{3t_{\rm fb}} \left(\frac{t}{t_{\rm fb}}\right)^{-5/3} \underset{M_{\rm acc}=0.4M_\star}{\approx} 1.1 \times 10^{26}\ \mathrm{g\ s^{-1}}\ M_{\bullet,6}^{-1/2} m_\star^{4/5} \left(\frac{t}{t_{\rm fb}}\right)^{-5/3}, \quad (3)$$

where $M_{\rm acc} \simeq 0.4 M_\star$ is the fraction of the star accreted at $t > t_{\rm fb}$ (the remainder $\sim 0.1\ M_\star$ being accreted during the rise phase at $t < t_{\rm fb}$; this fraction in general depends on the outer density structure of the star).

The peak Eddington ratio of the fallback rate,

$$\frac{\dot{M}_{\rm fb}(t_{\rm fb})}{\dot{M}_{\rm Edd}} \approx 65 M_{\bullet,6}^{-3/2} m_\star^{4/5}, \quad (4)$$

exceeds unity, where $\dot{M}_{\rm Edd} \equiv L_{\rm Edd}/(0.1c^2)$, $L_{\rm Edd} = 4\pi GM_\bullet c/\kappa_{\rm es} \approx 1.4 \times 10^{44} M_{\bullet,6}$ erg s$^{-1}$, and $\kappa_{\rm es} \approx 0.35$ cm$^2$ g$^{-1}$ is the electron scattering opacity.

Motivated by recent simulations (e.g., Andalman et al. 2022; Steinberg & Stone 2022), we assume rapid circularization of the initial tidal debris into a quasi-spherical envelope, on a timescale $t_{\rm circ} \sim t_{\rm fb}$. We further assume that the envelope possesses a power-law radial density profile with a characteristic radius $R_v$ and a sharp outer edge:

$$\rho = \frac{M_e}{4\pi R_v^3} \frac{(3-\xi)}{(7-2\xi)} \begin{cases} \left(\frac{r}{R_v}\right)^{-\xi} & r < R_v, \\ \exp\left[-(r-R_v)/R_v\right], & r > R_v, \end{cases} \quad (5)$$

where $\xi \lesssim 3$. In what follows we take $\xi = 1$, i.e., $\rho \propto r^{-1}$ for $r < R_v$;[3] however, the qualitative features of the model should be preserved for other choices $1 \lesssim \xi \lesssim 3$ (the "ZEBRA" models of Coughlin & Begelman 2014 predict $1/2 < \xi < 3$ for an adiabatic index $\gamma = 4/3$). Neglecting wind mass loss or SMBH accretion, the envelope mass grows with time $t > t_{\rm fb}$ as

$$M_e(t > t_{\rm fb}) = M_e(t_{\rm fb}) + \int_{t_{\rm fb}}^{t} \dot{M}_{\rm fb} dt' \underset{M_{\rm acc}=0.4M_\star}{\approx} 0.1 M_\star + 0.4 M_\star \left[1 - \left(\tfrac{t}{t_{\rm fb}}\right)^{-2/3}\right]. \quad (6)$$

We estimate the characteristic initial radius of the envelope $R_v$ ("virial radius") by equating the energy of the bound stellar debris, $|E_t| = kGM_\bullet M_\star R_\star/R_t^2$, to half of its gravitational binding energy $|E_b| = 4\pi \int GM_\bullet \rho r dr = 4GM_\bullet M_{\rm e}/5R_v$:

$$R_{v,0} \approx \tfrac{2R_\star}{5k} \left(\tfrac{M_\bullet}{M_\star}\right)^{2/3} \tfrac{M_e}{M_\star} \approx 6.8 \times 10^{13}\ \mathrm{cm}\ m_\star^{2/15} M_{\bullet,6}^{2/3} \left(\tfrac{M_{e,0}}{0.2M_\star}\right), \quad (7)$$

where in the second line and hereafter we take $k = 0.8$.

The envelope is notably much larger than the circularization radius, $R_{\rm circ} = 2R_t$,

$$\tfrac{R_{v,0}}{R_{\rm circ}} \approx \tfrac{\beta}{5k} \left(\tfrac{M_\bullet}{M_\star}\right)^{1/3} \tfrac{M_e}{M_\star} \approx 5.5 \beta m_\star^{-1/3} M_{\bullet,6}^{1/3} \left(\tfrac{M_{e,0}}{0.2M_\star}\right). \quad (8)$$

[3] Steinberg & Stone (2022) found $\rho \propto r^{-1.3}$ out to a break radius $R_b \sim 10^{14}$ cm and $\rho \propto r^{-4}$ at $r \gg R_b$ (E. Steinberg 2022, private communication).

Rotational support is thus subdominant initially compared to thermal pressure, rendering the envelope quasi-spherical. The envelope energy we assume is smaller (equivalently, $R_v$ is larger) than that of Loeb & Ulmer (1997), who, in adopting a steeper density profile $\rho \propto r^{-3}$, effectively take $R_v \sim R_{\rm circ}$ (their Equation (14)), a more tightly bound envelope than imparted by the TDE.

The characteristic density of the envelope at $r = R_v$ is given by

$$\rho_c \equiv \rho(R_v) = \frac{M_e}{10\pi R_v^3} \approx 4 \times 10^{-11} {\rm g\ cm^{-3}} m_\star^{3/5} \times M_{\bullet,6}^{-2} \left(\frac{M_e}{0.2M_\star}\right)^{-2} \left(\frac{R_v}{R_{v,0}}\right)^{-3}. \quad (9)$$

From the virial theorem, the envelope's internal energy $E_{\rm int} = 3\int P_{\rm rad} 4\pi r^2 dr \equiv 4\pi R_v^3 \bar{P}_{\rm rad}$ equals $|E_t|$, leading to an estimate of the interior temperature:

$$T_c \equiv \left(\frac{3\bar{P}_{\rm rad}}{a}\right)^{1/4} = \left(\frac{3GM_eM_\bullet}{10\pi a R_v^4}\right)^{1/4} \approx 4.2 \times 10^5 {\rm\ K}\, m_\star^{7/60} \times \times M_{\bullet,6}^{-5/12} \left(\frac{M_e}{0.2M_\star}\right)^{-3/4} \left(\frac{R_v}{R_{v,0}}\right)^{-1}. \quad (10)$$

Thus, as the envelope contracts and $R_v$ decreases, both $\rho_c$ and $T_c$ will rise. Radiation pressure $P_{\rm rad} = aT^4/3$ dominates over gas pressure $P_{\rm gas} = \rho kT/\mu m_p$ at all times:

$$\frac{P_{\rm rad}}{P_{\rm gas}} \sim 10^4 \left(\frac{T_c}{10^5\ {\rm K}}\right)^3 \left(\frac{\rho_c}{10^{-11}\ {\rm g\ cm^{-3}}}\right)^{-1} \propto R_v^0. \quad (11)$$

For $\rho \propto r^{-\xi}$, hydrostatic balance $dP_{\rm rad}/dr \propto -GM_\bullet \rho/r^2$ implies $T \propto r^{-(1+\xi)/4}$, and hence our assumed density profile ($\xi = 1$; Equation (5)) implies $T \propto r^{-1/2}$. The envelope entropy profile $s \propto T^3/\rho \propto r^{(\xi-3)/4}$ is therefore unstable to convection ($ds/dr < 0$). While efficient convection may try to drive $s \simeq$ const ($\rho \propto r^{-3}$), for $\xi = 3$ such a configuration would be more tightly gravitationally bound than permitted by its initial energy. The envelope structure may therefore try to evolve toward $\xi = 3$ as it cools and contracts, but for simplicity we neglect this possibility and assume $\xi = 1$ in our fiducial model setup and analytic estimates (though we do explore the impact of adopting a larger value of $\xi = 2$ on the light-curve evolution).

### 2.2. Envelope Evolution

After forming at time $t_{\rm circ} \approx t_{\rm fb}$, the mass and energy,

$$|E| = \frac{1}{2}|E_b| = \frac{2GM_\bullet M_e}{5R_v} \quad (12)$$

(and hence characteristic radius $R_v$), of the envelope evolve at later times according to

$$\frac{dM_e}{dt} = \dot{M}_{\rm fb} - \dot{M}_\bullet - \dot{M}_w, \quad (13)$$

$$\frac{d|E|}{dt} = L_{\rm Edd} - \dot{E}_\bullet + \dot{E}_w, \quad (14)$$

respectively. Here $\dot{M}_\bullet/\dot{E}_\bullet$ accounts for the effects of accretion onto the SMBH, a specific treatment of which is given in Sections 2.2.1. The terms $\dot{M}_w/\dot{E}_w$ allow for mass loss and energy loss in a wind from the envelope given an appropriate prescription relating them to other properties of the system. Though included for completeness, we neglect outflows hereafter (i.e., we take $\dot{M}_w = \dot{E}_w = 0$); we speculate on when this assumption may be violated in Section 4.

The luminosity radiated by the envelope can be written as

$$L_{\rm rad} \simeq L_{\rm Edd} + L_{\rm fb} = 4\pi\sigma T_{\rm eff}^4 R_{\rm ph}^2, \quad (15)$$

where $T_{\rm eff}$ and $R_{\rm ph}$ are the effective temperature and photosphere radius, respectively.[4] The latter is defined by

$$\tau = \int_{R_{\rm ph}}^{\infty} \kappa\rho dr = 1. \quad (16)$$

For our assumed density profile at $r > R_v$ (Equation (5)),

$$R_{\rm ph} = R_v(1 + \ln\Lambda), \quad (17)$$

where the characteristic optical depth

$$\Lambda \equiv \frac{\kappa M_e}{10\pi R_v^2} \approx 960\, m_\star^{-4/15} \times M_{\bullet,6}^{-4/3} \left(\frac{\kappa}{\kappa_{\rm es}}\right) \left(\frac{M_{e,0}}{0.2M_\star}\right)^{-1} \left(\frac{R_v}{R_{v,0}}\right)^{-2}, \quad (18)$$

and we hereafter take $\kappa = \kappa_{\rm es} \simeq 0.35$ cm$^2$ g$^{-1}$ (scattering generally dominates other opacity sources given the envelope's high entropy).

The envelope is in hydrostatic equilibrium and supported by radiation pressure, so its inner layers must radiate close to the SMBH Eddington luminosity, $L_{\rm Edd} \approx 1.4 \times 10^{44} M_{\bullet,6}$ erg s$^{-1}$ (Loeb & Ulmer 1997), which therefore enters as a loss term in Equation (14). The second term in Equation (15),

$$L_{\rm fb} = \frac{GM_\bullet \dot{M}_{\rm fb}}{R_{\rm acc}}, \quad (19)$$

accounts for heating of the outer envelope layers by the fallback stream (specific kinetic energy $v_{\rm ff}^2/2 \approx GM_\bullet/r$ at radius $r$), where $r \sim R_{\rm acc}$ is the characteristic radius at which the the stream material decelerates and becomes incorporated into the envelope.[5]

Steinberg & Stone (2022) show that the densest portion of the fallback stream—that which remains gravitationally self-bound—thickens during compression at pericenter and then dissolves into the envelope on a radial scale $\sim R_{v,0}$ (as a part of the same process giving rise to efficient circularization in the first place). Bonnerot et al. (2016a) also find that Kelvin–Helmholtz instabilities acting on a debris stream passing through an ambient gaseous medium are most severe near apocenter. Motivated thus, we assume that the accretion radius scales with the apocenter distance of the fallback stream,

$$R_{\rm acc} = \zeta R_{v,0} \left(\frac{t}{t_{\rm fb}}\right)^{2/3}, \quad (20)$$

[4] We neglect the fact that for a scattering-dominated atmosphere the thermalization surface can be deeper than the photosphere, changing the relationship between effective temperature and the scattering photosphere radius (e.g., Lu & Bonnerot 2020; Steinberg & Stone 2022).

[5] By including $L_{\rm fb}$ in $L_{\rm rad}$ (Equation (15)) but not Equation (14), we have implicitly assumed that $L_{\rm fb}$ is "instantaneously" radiated by the envelope. This is generally a good assumption because the timescale over which $L_{\rm fb}$ evolves $\sim t$ is typically long compared to the Kelvin–Helmholtz time over which the envelope can radiate any deposited energy (see Equation (29)).

where the constant $\zeta$ accounts for various uncertainties (e.g., in the radial distribution of the envelope heating and the fraction of the stream able to penetrate the envelope). We adopt a fiducial value $\zeta = 2$, because only the fraction (e.g., $\sim 1/2$, depending on $\beta$; Steinberg et al. 2019) of the stream mass confined in the transverse directions by self-gravity (e.g., Coughlin et al. 2016) is likely to survive penetration through the envelope to radii $\sim R_v$. At late times $R_{\rm acc}$ can grow to exceed the envelope radius, which motivates capping the value of $R_{\rm acc}$ at $R_v$; however, insofar that fallback heating generally contributes only moderately to the luminosity at these late times, our light-curve predictions are insensitive to this choice, and so we adopt the simpler prescription given by Equation (20).

#### 2.2.1. Black Hole Accretion

Insofar as the envelope retains the same specific angular momentum from the time of disruption, rotation will become important on small radial scale $\lesssim R_{\rm circ} = 2R_p = 2R_t/\beta \ll R_v$, thus limiting accretion onto the SMBH based on the viscous time at this radius. We estimate the accretion rate through the rotationally supported inner disk region (second term in Equation (13)) as

$$\dot{M}_\bullet \simeq 3\pi\nu\Sigma|_{R_{\rm circ}} \equiv \frac{M_e}{t_{\rm acc}}, \tag{21}$$

where $\Sigma \simeq \rho(R_{\rm circ})R_{\rm circ} \simeq M_e/(10\pi R_v^2)$, $\nu = \alpha c_s^2/\Omega = r^2\Omega(H/r)^2$, $\alpha$ is the Shakura & Sunyaev (1973) viscosity parameter, $H/r = c_s/(r\Omega)$ is the vertical disk aspect ratio, $c_s = (P/\rho)^{1/2}$ is the sound speed, and $\Omega = (GM_\bullet/r^3)^{1/2}$ is the Keplerian orbital frequency. An "accretion" timescale for the envelope can thus be defined,

$$t_{\rm acc} = \frac{10}{3\alpha}\frac{R_v^2}{(GM_\bullet R_{\rm circ})^{1/2}}\left(\frac{H}{r}\right)^{-2} \approx 12.8\ {\rm yr}\ \frac{\beta^{1/2}}{\alpha_{-2}} \times m_\star^{1/30} M_{\bullet,6}^{2/3}\left(\frac{H}{0.3r}\right)^{-2}\left(\frac{M_{e,0}}{0.2M_\star}\right)^2\left(\frac{R_v}{R_{v,0}}\right)^2, \tag{22}$$

where $\alpha_{-2} \equiv \alpha/(10^{-2})$ and we are motivated to consider a geometrically thick disk $H/r \gtrsim 0.3$, consistent with the near-Eddington accretion rates of interest. Though initially much longer than other timescales in the problem, $t_{\rm acc}$ will shorten $\propto R_v^2$ as the envelope cools and contracts.

Finally, the third term in Equation (14) accounts for energy released by accretion onto the SMBH that is transferred outward to the envelope through radiation or convection. We assume that the feedback luminosity scales with the accretion rate at $R_{\rm circ}$,

$$\dot{E}_\bullet = \eta\dot{M}_\bullet c^2, \tag{23}$$

where the dimensionless efficiency $\eta \lesssim 0.1$ encapsulates a number of uncertain factors related to efficiency of reprocessing by the envelope of radiation/outflows/jets from the inner disk, including the potential for disk-wind mass loss from the (potentially super-Eddington) accretion flow between $R_{\rm circ}$ and $R_{\rm isco}$ (e.g., Blandford & Begelman 1999). A canonical minimum value, set by the condition $\dot{E}_\bullet = GM_\bullet\dot{M}_\bullet/R_{\rm circ}$, is

$$\eta_{\rm min} = \frac{R_g}{R_{\rm circ}} \approx 10^{-2}\beta m_\star^{-7/15} M_{\bullet,6}^{2/3}. \tag{24}$$

**Table 1**
Model Parameters

| Symbol | Description | Fiducial Value |
|---|---|---|
| $M_\star = m_\star M_\odot$ | Star mass | $1\ M_\odot$ |
| $M_\bullet$ | SMBH mass | $2\times10^6\ M_\odot$ |
| $\beta \equiv R_t/R_p$ | Orbit penetration factor | 1 |
| $\xi$ | Envelope density power law (Equation (5)) | 1 |
| $\zeta$ | Stream penetration factor (Equation (20)) | 2 |
| $\alpha$ | Viscosity parameter (Equation (22)) | $10^{-2}$ |
| $H/r$ | Disk aspect ratio (Equation (22)) | 0.3 |
| $\eta \equiv \dot{E}_\bullet/(\dot{M}_\bullet c^2)$ | SMBH feedback efficiency (Equation (23)) | $10^{-2}$ |

### 2.3. Summary of the Model

As summarized in Table 1, a given model is defined primarily by the masses of the star $M_\star$ and SMBH $M_\bullet$. Secondary variables, whose values we shall typically fix within a fiducial value or range, include the following: orbital penetration factor $\beta = 1$, density radial profile power law $\xi = 1$–2, fallback heating efficiency $\zeta = 2$, viscosity $\alpha = 0.01$, aspect ratio $H/r = 0.3$, and feedback efficiency $\eta \sim \eta_{\rm min} \sim 10^{-2} - 10^{-1}$ of the inner accretion disk. Starting the calculation at time $t = t_{\rm fb}$, when the envelope mass $M_e(t_0) = 0.1M_\star$ (Equation (6)) and radius $R_v = R_{v,0}$ (Equation (7)), we solve Equations (13) and (14) for the evolution of $M_e$, radius $R_v$, photosphere radius $R_{\rm ph}$, and effective temperature $T_{\rm eff}$ of the envelope, as well as the SMBH accretion rate $\dot{M}_\bullet$.

We evolve the system until the envelope mass reaches zero, though the assumptions of the model may break down before this, once the radius contracts to $R_v \lesssim R_{\rm circ} = 2R_t/\beta$, violating the assumption of negligible rotational support. Given the bolometric luminosity $L_{\rm rad}$ and $T_{\rm eff}$, we calculate the luminosity $\nu L_\nu$ at a given optical wave band $\nu$ assuming blackbody emission (e.g., we neglect the distinction between the scattering photosphere and frequency-dependent thermalization surface, which can lead to an underestimate of the luminosity on the Rayleigh–Jeans tail; e.g., Lu & Bonnerot 2020).

## 3. Results

We begin in Section 3.1 by showing results for a fiducial model with $M_\star = M_\odot$, $M_\bullet = 2\times10^6\ M_\odot$, $\beta = 1$. Rather than including all of the physics in the model at once, we begin (Section 3.1.1) by artificially neglecting the effects arising from accretion onto the SMBH (i.e., we assume $\dot{M}_\bullet = \dot{E}_\bullet = 0$) and walking through some analytic arguments that reproduce the results. Then, we move on to models that include SMBH accretion, first just a mass-loss term for the envelope (Section 3.1.2) and then finally including also SMBH energy feedback (Section 3.1.3). Finally, Section 3.2 presents the full-model optical/X-ray light curves for a range of star and SMBH properties.

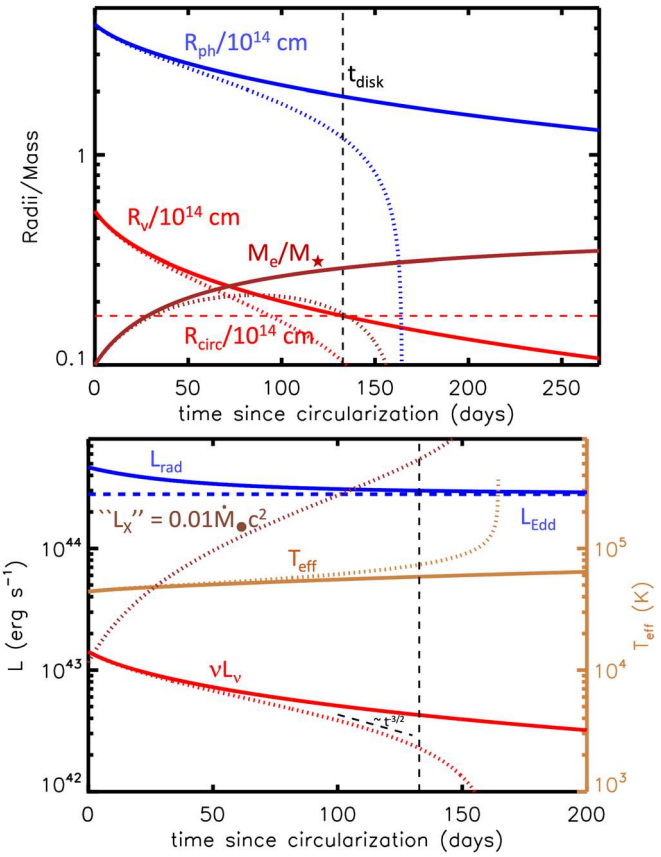


**Figure 2.** Evolution of TDE cooling envelope model with $M_\star = M_\odot$, $M_\bullet = 2 \times 10^6\ M_\odot$, $\beta = 1$, shown as a function of time since the circularization/envelope assembly time $t = t_{\rm fb}$. Solid lines show a model neglecting mass accretion onto the SMBH (i.e., $\dot{M}_\bullet = \dot{E}_\bullet = 0$), while dotted lines show the effects of including SMBH accretion mass loss (Equation (21) for $\alpha = 0.01$, $H/r = 0.3$) but not energy feedback. The top panel shows the characteristic envelope radius $R_v$, mass $M_e/M_\star$, and photosphere radius $R_{\rm ph}$, while the bottom panel shows the envelope luminosity $L_{\rm rad}$, optical luminosity $\nu L_\nu$ at frequency $\nu = 6 \times 10^{14}$ Hz ($g$ band), effective temperature $T_{\rm eff}$, and $L_{\rm X} \equiv 0.01 M_\bullet c^2$, taken as a proxy for the X-ray luminosity from the inner disk (potentially observable only through a narrow polar region). The envelope evolution concludes roughly once $R_v$ decreases to $R_{\rm circ}$ (horizontal dashed line), as occurs roughly at the times $t_{\rm disk}$ (Equation (33)) and $t^\star_{\rm acc}$ (Equation (34)), respectively, in the two models. A dashed black line illustrates $\propto t^{-3/2}$ decay.

### 3.1. Fiducial Model

#### 3.1.1. Pure Cooling (Kelvin–Helmholtz Contraction)

Solid lines in Figure 2 show results for the envelope evolution, neglecting accretion or feedback onto the SMBH. The envelope radius $R_v$ and photosphere radius $R_{\rm ph}$ begin large but gradually decay with time, with $R_v$ reaching $R_{\rm circ}$ by around day 130 measured with respect to the envelope assembly (time $t_{\rm circ} \sim t_{\rm fb}$ after the disruption). Likewise, while the bolometric luminosity is at or slightly above the Eddington luminosity of the SMBH at all times, the optical decays from its initial value $\nu L_\nu \gtrsim 10^{43}$ erg s$^{-1}$ roughly $\propto t^{-3/2}$, as the effective temperature rises. These results can largely be understood analytically.

Neglecting fallback heating, Equation (14) becomes

$$\frac{2GM_\bullet M_e}{5R_v^2}\frac{dR_v}{dt} = L_{\rm Edd}(M_\bullet). \tag{25}$$

Further approximating the envelope mass $M_e$ as a constant (in reality, $M_e$ grows gradually to $0.5M_\star$), we obtain

$$\frac{2GM_\bullet M_e}{5}\left(\frac{1}{R_v} - \frac{1}{R_{v,0}}\right) = L_{\rm Edd} t. \tag{26}$$

The radius contracts as

$$\frac{R_v}{R_{v,0}} = \left(1 + \frac{5L_{\rm Edd} t R_{v,0}}{2GM_\bullet M_{\rm env}}\right)^{-1} = \left(1 + \frac{t}{t_{\rm KH,0}}\right)^{-1}, \tag{27}$$

where

$$t_{\rm KH} \equiv \frac{2GM_\bullet M_e}{5L_{\rm Edd}R_v} \simeq 24\ d\ m_\star^{13/15} M_{\bullet,6}^{-2/3}\left(\frac{R_v}{R_{v,0}}\right)^{-1} \tag{28}$$

is the "Kelvin–Helmholtz" time and $t_{\rm KH,0} = t_{\rm KH}(R_v = R_{v,0})$ defines its initial value.[6] Making use of Equation (2), we see that

$$\frac{t_{\rm KH}}{t} \approx 0.41\ m_\star^{2/3} M_{\bullet,6}^{-7/6}\left(\frac{R_v}{R_{v,0}}\right)^{-1}\left(\frac{t}{t_{\rm fb}}\right)^{-1}. \tag{29}$$

The fact that $t_{\rm KH}/t \ll 1$ at times $t \gtrsim t_{\rm fb} \sim t_{\rm circ}$ implies that (1) thermal equilibrium can be established on the timescale the envelope is being assembled and will remain so at later times, and (2) if the assembly process itself is not rapid (taking place over a timescale $\gtrsim$0.1–1 $t_{\rm fb}$, depending on the SMBH mass), then the light-curve properties near peak light will depend on the assembly history and hence may not be captured by our model, which assumes instantaneous assembly (we return to this point in Section 3.2).

Figure 2 shows that the envelope luminosity (Equation (15)) roughly obeys $L_{\rm rad} \simeq L_{\rm Edd}$ with the fallback luminosity $L_{\rm fb}$ (Equation (19)) boosting this value only moderately at early times. Indeed, from Equations (3), (20), and (27) we obtain

$$\frac{L_{\rm fb}}{L_{\rm Edd}} \simeq \frac{GM_\bullet \dot{M}_{\rm fb}}{R_{\rm acc}L_{\rm Edd}} \approx \frac{GM_\bullet \dot{M}_{\rm fb}}{\zeta R_v L_{\rm Edd}} \underset{t \gg t_{\rm KH,0}}{\approx} 0.7\left(\frac{\zeta}{2}\right)^{-1}\left(\frac{M_{e,0}}{0.2M_\star}\right)^{-1}\left(\frac{t}{t_{\rm fb}}\right)^{-4/3}, \tag{30}$$

a result that is notably independent of $m_\star$ and $M_\bullet$. Fallback accretion thus contributes at an order-unity level to the envelope luminosity at early times $t \sim t_{\rm fb}$ but becomes comparatively less important with time relative to the passive envelope cooling.

Approximating $L_{\rm rad} \simeq L_{\rm Edd}$ and using Equations (15), (17), and (27), the effective temperature evolves according to

$$T_{\rm eff} \simeq \left(\frac{L_{\rm Edd}}{4\pi\sigma R_{\rm ph}^2}\right)^{1/4} \simeq 4.5 \times 10^4\ {\rm K}\ m_\star^{-1/15} \times M_{\bullet,6}^{-1/12}\left(\frac{M_{e,0}}{0.2\ M_\odot}\right)^{-1/2}\left(\frac{\ln\Lambda}{10}\right)^{-1/4}\left(1 + \frac{t}{t_{\rm KH,0}}\right)^{1/2}. \tag{31}$$

The predicted gradual rise in $T_{\rm eff} \propto t^{1/2}$ is consistent with that shown in Figure 2 and similar to that of observed TDE UV/optical flares (e.g., van Velzen et al. 2021a, their Figure 5).

[6] The thermal timescale $t_{\rm KH}$ also equals the photon diffusion time through the envelope, $t_{\rm diff} \sim \Lambda(R_v/c)$, where $\Lambda$ is the characteristic optical depth (Equation (18)).

The optical luminosity, in the Rayleigh–Jeans approximation $h\nu \ll kT_{\rm eff}$, evolves as

$$\nu L_\nu \simeq \frac{8\pi^2}{c^2}\nu^3 kT_{\rm eff}R_{\rm ph}^2$$
$$\simeq 5.4\times 10^{43}{\rm erg\ s^{-1}}\left(\frac{\nu}{6\times 10^{14}\ {\rm Hz}}\right)^3 m_\star^{1/5}$$
$$\times M_{\bullet,6}^{5/4}\left(\frac{M_{e,0}}{0.2M_\star}\right)^{3/2}\left(\frac{\ln\Lambda}{10}\right)^{7/4}\left(1+\frac{t}{t_{\rm KH,0}}\right)^{-3/2}, \quad (32)$$

again in reasonable agreement with Figure 2. The predicted $\propto t^{-3/2}$ power-law decay is (coincidentally) similar to the mass fallback rate, $\dot{M}_{\rm fb}\propto t^{-5/3}$ (Equation (3)).

Envelope contraction as we have modeled it will continue until rotational support becomes important, as occurs once $R_\nu$ decreases to $R_{\rm circ}=2R_t$. Again neglecting accretion onto the SMBH, this timescale for the envelope to transform into a disk can be estimated using Equation (27) (in the $t\gg t_{\rm KH,0}$ limit):

$$t_{\rm disk}\simeq\frac{R_{\nu,0}}{2\beta R_t}t_{\rm KH,0}\simeq\frac{1}{5\beta}\frac{GM_\bullet M_{e,0}}{L_{\rm Edd}R_t}$$
$$\approx 121\ d\ m_\star^{8/15}M_{\bullet,6}^{-1/3}, \quad (33)$$

i.e., typically several months to a year, in agreement with where $R_\nu$ crosses $R_{\rm circ}$ in Figure 2.

### 3.1.2. Mass Loss from SMBH Accretion

A dotted line in Figure 2 shows an otherwise identical model to that presented in the previous figure, but which now includes envelope mass loss due to SMBH accretion (Equation (21), assuming $\alpha=10^{-2}$ and $H/r=0.3$) yet still neglects any feedback heating from the accretion. At early times the solution is similar to that neglecting accretion, until around day 100, when the envelope mass reaches a maximum and begins to decrease. This in turn drives $R_\nu$ and $R_{\rm ph}$ to decrease, and thus $T_{\rm eff}$ to increase and $\nu L_\nu$ to drop, at a faster rate than they would otherwise without accretion.

We can estimate the time required for the envelope to be fully accreted by setting $t=t_{\rm acc}$ (Equation (22)) with $R_\nu \underset{t\gg t_{\rm KH,0}}{=} R_{\nu,0}(t_{\rm KH,0}/t)$ (Equation (27)), which gives

$$t_{\rm acc}^\star\simeq\frac{0.72}{\alpha^{1/3}}\left(\frac{H}{r}\right)^{-2/3}\frac{(GM_\bullet)^{1/2}M_{e,0}^{2/3}}{L_{\rm Edd}^{2/3}R_{\rm t}^{1/6}}\approx 146\ {\rm days}\ \alpha_{-2}^{-1/3}$$
$$\times\left(\frac{H}{0.3r}\right)^{-2/3}m_\star^{53/90}M_{\bullet,6}^{-2/9}\left(\frac{M_{e,0}}{0.2M_\star}\right)^{2/3}, \quad (34)$$

in rough agreement with where $M_e$ begins to fall rapidly in Figure 2. Depending on the value of $\alpha(H/r)^2$, $t_{\rm acc}^\star$ can be larger or smaller than $t_{\rm disk}$, the maximum disk formation time absent accretion (Equation (33)).

Accretion onto the central SMBH can in principle power X-ray emission, which may begin to escape along what may be a narrow accretion funnel (e.g., Dai et al. 2018; Kara et al. 2018) to a greater and greater fraction of external observers as the envelope becomes more disk-like ($R_\nu\rightarrow R_{\rm circ}$). A brown dotted line in Figure 2 shows an estimate of this proxy X-ray luminosity,

$$L_{\rm X}\equiv 10^{-2}\dot{M}_\bullet c^2, \quad (35)$$

where the prefactor $10^{-2}$ is an estimate of the radiative efficiency of super-Eddington accretion disks (e.g., Sadowski & Narayan 2016). Although the normalization of the X-ray power is clearly uncertain and the observed luminosity is highly inclination dependent (e.g., Dai et al. 2018), the key feature of note is the *delayed rise* of the X-ray light curve relative to the optical peak. Though such delayed X-ray rises are observed in some TDEs, they have frequently been attributed to inefficient or delayed circularization (e.g., Shiokawa et al. 2015; Gezari et al. 2017). The physics here is instead *delayed cooling* and envelope contraction, which leads to accelerating growth in the SMBH accretion rate $\dot{M}_\bullet\propto t_{\rm acc}^{-1}\propto R_\nu^{-2}$ (Equation (22)).

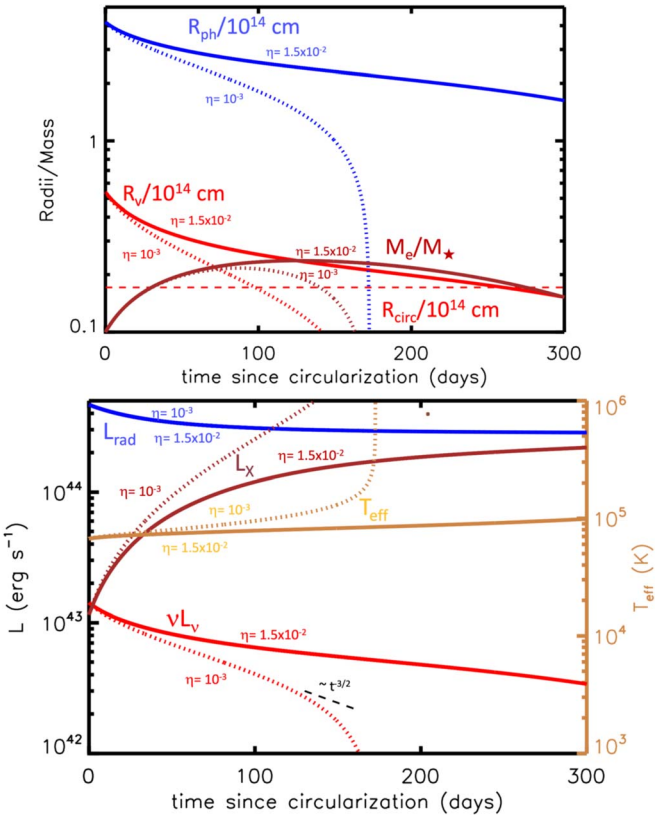


**Figure 3.** Models calculated for the same parameters as in Figure 3, but now including the effects of SMBH feedback on the envelope structure for two different values of $\eta=1.5\times10^{-2}$ (solid lines) and $\eta=10^{-3}$ (dotted lines). Powerful feedback (large $\eta$) acts to slow the rate of envelope cooling and accretion, flattening the late-time $\nu L_\nu$ optical light-curve decay. A dashed black line shows $\propto t^{-3/2}$ decay, as roughly expected absent efficient feedback.

### 3.1.3. Feedback from SMBH Heating

Finally, in Figure 3 we show the effects of adding SMBH accretion heating to the envelope evolution (Equation (23)), by comparing a model with a low feedback efficiency $\eta=10^{-3}$ (dotted line) to one with higher efficiency $\eta=1.5\times10^{-2}$ (solid line). The $\eta=10^{-3}$ model follows a similar evolution to models excluding feedback altogether (Figure 2). However, the $\eta=1.5\times10^{-2}$ model differs markedly, exhibiting a much more gradual decline in the rate of envelope contraction and optical luminosity. In effect, the energy provided by SMBH accretion keeps the envelope "puffed up" for longer, which in turn slows the SMBH accretion rate.

This regulated state, in which SMBH feedback reaches a balance with the radiated luminosity $L_{\rm rad}\simeq L_{\rm Edd}$, can be expressed as a condition on the SMBH accretion rate (see also

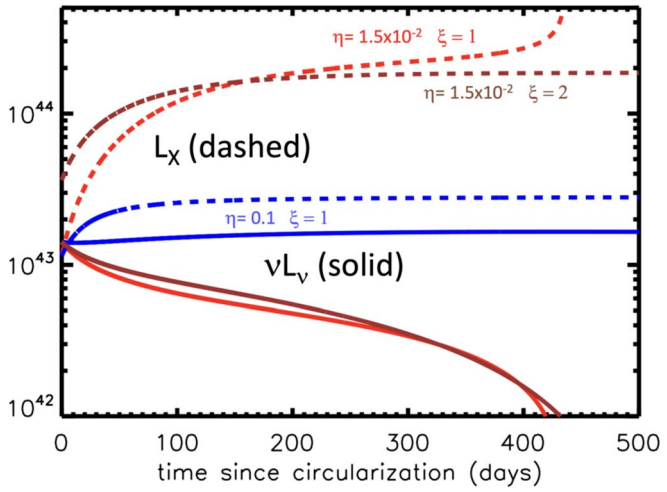


**Figure 4.** Optical-band light curves $\nu L_\nu$ at $\nu = 6 \times 10^{14}$ Hz and proxy X-ray light curves $L_X = 10^{-2}\dot{M}_\bullet c^2$ for a series of models that adopt fiducial parameters ($M_\star = M_\odot$, $M_\bullet = 2 \times 10^6\, M_\odot$, $\beta = 1$, $\alpha = 10^{-2}$, $H/r = 0.3$, $\zeta = 2$) but varying the SMBH feedback parameter $\eta$ and envelope power-law density index $\xi$ as marked.

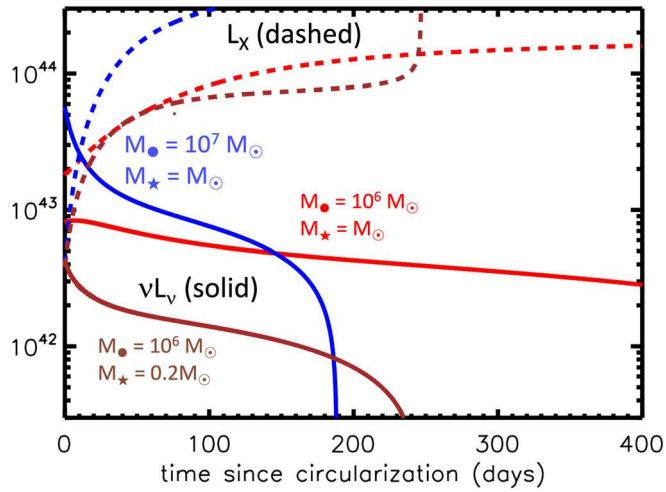


**Figure 5.** Optical-band light curves $\nu L_\nu$ at $\nu = 6 \times 10^{14}$ Hz and proxy X-ray light curves $L_X = 10^{-2}\dot{M}_\bullet c^2$ for a series of models that adopt fiducial parameters ($\beta = 1$, $\alpha = 10^{-2}$, $H/r = 0.3$, $\zeta = 2$) but varying the mass of the star and SMBH as marked. We assume an SMBH feedback parameter $\eta = \eta_{\rm min}(M_\star, M_\bullet)$. (Equation (24)).

Loeb & Ulmer 1997)

$$\dot{E}_\bullet \simeq L_{\rm Edd} \Rightarrow \dot{M}_\bullet = \frac{L_{\rm Edd}}{\eta c^2}. \quad (36)$$

Equating this with Equation (21), the corresponding envelope radius in the SMBH-regulated state is given by

$$R_{\rm v}^\bullet \simeq \left(\frac{3\eta\alpha c^2}{10}\left(\frac{H}{r}\right)^2 \frac{M_e}{L_{\rm Edd}}\right)^{1/2} (GM_\bullet R_{\rm circ})^{1/4}$$
$$\approx 1.7 \times 10^{13}{\rm cm}\, \frac{\eta_{-2}^{1/2}\alpha_{-2}^{1/2}}{\beta^{1/4}}\left(\frac{H}{0.3r}\right) m_\star^{37/60} M_{\bullet,6}^{-1/6}\left(\frac{M_e}{0.2M_\star}\right)^{1/2} \quad (37)$$

The timescale for the envelope to be completely accreted at the regulated rate (Equation (36)) is thus given by

$$t_{\rm acc}^\bullet = \frac{M_e}{\dot{M}_\bullet} = \frac{\eta M_e c^2}{L_{\rm Edd}} \simeq 300\, d\, \eta_{-2} m_\star M_{\bullet,6}^{-1}\left(\frac{M_e}{0.2M_\star}\right) \quad (38)$$

From when $R_v$ decreases from its initial value to $R_v^\bullet$ until the time the envelope is accreted $t \sim t_{\rm acc}^\bullet$, the envelope radius and optical luminosity will exhibit a flat plateau-like time evolution (suggestive of the late-time behavior of some TDE light curves; e.g., Leloudas et al. 2016; van Velzen et al. 2019; Wevers et al. 2019).

The regulated plateau state can only be achieved if $t_{\rm acc}^\bullet > t_{\rm acc}^\star$, as occurs for sufficiently high accretion feedback efficiency,

$$\eta > \eta_{\rm crit} \approx 5 \times 10^{-3}\alpha_{-2}^{-1/3}\left(\frac{H}{0.3r}\right)^{-2/3} \times$$
$$m_\star^{-37/90} M_{\bullet,6}^{7/9}\left(\frac{M_e}{0.2M_\star}\right)^{-1/3}, \quad (39)$$

consistent with the large difference in the light-curve duration between the $\eta = 1.5 \times 10^{-2}$ and $\eta = 10^{-3}$ models in Figure 3. For fiducial values of $\alpha$ and $H/r$, $\eta_{\rm crit}$ is comparable to $\eta_{\rm min}$ (Equation (24)); this suggests that events both with and without a self-regulated plateau phase could occur among the TDE population depending on the precise system parameters.

Figure 4 shows the optical $\nu L_\nu$ and proxy X-ray $L_X = 10^{-2}\dot{M}_\bullet c^2$ light curves of the fiducial model compared to otherwise identical calculations with higher feedback efficiency $\eta = 0.1$ and larger envelope density power-law index $\xi = 2$. More efficient SMBH feedback slows the envelope contraction and flattens the optical light curve even from early times, and it reduces the SMBH accretion rate (proxy X-ray light curve). The envelope and light-curve evolution depends only weakly on $\xi$, except at the end of the evolution, when the accretion rate abruptly rises for the $\xi = 1$ model but not $\xi = 2$; however, insofar as this abrupt rise occurs at the same time $R_v$ is approaching $R_{\rm circ}$ and hence an assumption of a pressure-supported envelope is breaking down, the robustness of this temporal feature is already somewhat questionable.

### 3.2. Dependence on SMBH/Star Properties

Figure 5 shows the optical $\nu L_\nu$ and X-ray $L_X$ light curves for a series of models that adopt fiducial parameters but varying the star and SMBH mass as marked and fixing $\eta = \eta_{\rm min}(M_\star, M_\bullet)$ (Equation (24)). The optical luminosity is higher for more massive stars or SMBHs, consistent with Equation (32). TDEs of lower-mass stars and/or by higher-mass SMBHs also tend to produce faster-decaying optical light curves (and correspondingly faster-rising proxy X-ray light curves), as expected because of their shorter envelope cool times (Equation (28)). Since $\eta_{\rm min} \gtrsim \eta_{\rm crit}$ for the assumed values of $\{\beta, \alpha, H/r\}$, the total light-curve durations (400, 150, and 250 days, respectively) are boosted moderately by SMBH feedback, roughly in accord with the scalings $t_{\rm acc}^\bullet \propto m_\star^{8/15} M_\bullet^{-1/3}$ (Equation (38)).

Van Velzen et al. (2021a, hereafter V21) analyze the optical light-curve properties of a sample of 17 TDEs detected by the Zwicky Transient Facility, exploring internal correlations between the light-curve properties (e.g., blackbody luminosity $L_{\rm rad}$, blackbody [our photosphere] radius $R_{\rm ph}$, effective temperature $T_{\rm eff}$, rise time $t_{\rm rise}$, decay time $t_{\rm decay}$) and with the host galaxy stellar mass $M_{\rm gal}$ (a rough proxy for the SMBH mass given $M_{\rm gal}$–$M_\bullet$ and related correlations; e.g., Magorrian et al. 1998). We briefly comment on our model's predictions in terms of their findings.

Albeit with large scatter, V21 find evidence for a positive correlation between the blackbody luminosity and host galaxy

mass. This supports more luminous TDEs arising from higher-mass SMBHs, consistent with the Eddington-limited luminosity $L_{\rm rad} \propto L_{\rm Edd}$ of a hydrostatic envelope (as predicted in our model given the likely subdominant role played by fallback accretion luminosity throughout the bulk of the light curve; Equation (30)).

V21 also find that the flare rise time is correlated with peak luminosity and anticorrelated with the photosphere radius. Insofar as $t_{\rm rise}$ is set by the timescale of envelope assembly $\sim t_{\rm circ}$ (e.g., Steinberg & Stone 2022), it could be expected to scale with the fallback time (Equation (2)), i.e.,

$$t_{\rm rise} \sim t_{\rm circ} \sim t_{\rm fb} \propto m_\star^{1/5} M_\bullet^{1/2}, \quad (40)$$

leading to a correlation between $t_{\rm rise} \propto M_\bullet^{1/2} \propto L_{\rm rad}^{1/2}$.

The situation regarding the light-curve decay time is more complicated. At face value our model predicts that the initial decay time should scale with the initial envelope cooling time (Equation (28)), i.e.,

$$t_{\rm decay} \propto t_{\rm KH,0} \propto m_\star^{2/3} M_\bullet^{-7/6}, \quad (41)$$

thus predicting a negative correlation between $t_{\rm decay}$ and $M_\bullet$ and hence between $t_{\rm decay}$ and $M_{\rm gal}$, contradicting the positive correlation found by V21. However, as already mentioned, because $t_{\rm KH,0}/t_{\rm fb} < 1$ (Equation (29)), the light-curve shape near peak may be influenced by the envelope assembly processes if the process is not sufficiently abrupt (assembly duration $\ll t_{\rm fb}$). A significant contribution from fallback heating at $t \sim t_{\rm fb}$ (Equation (30)) could also imprint some $t_{\rm fb}$ dependence into the early light-curve decay. Finally, feedback heating from the SMBH also acts to flatten the light curve and increase $t_{\rm decay}$ and may become more efficient for higher SMBH masses because the circularization radius is typically deeper within the gravitational potential well.

The strongest correlation found by V21 is between $L_{\rm pk}/R_{\rm ph}$ and $t_{\rm rise}$. Taking $L_{\rm pk} \propto M_\bullet$ and $R_{\rm ph} \propto R_\nu \propto m_\star^{2/15} M_\bullet^{2/3}$ and eliminating the SMBH mass, our model would predict

$$\frac{L_{\rm pk}}{R_{\rm ph}} \propto m_\star^{-2/15} M_\bullet^{1/3} \propto m_\star^{-4/15} t_{\rm rise}^{2/3}. \quad (42)$$

While the weak dependence on stellar mass is encouraging for generating a tight correlation, the scaling with $t_{\rm rise}$ is somewhat too shallow compared to the data (V21, their Figure 9).

Our model dictates a minimum evolution timescale for TDE optical light curves set by the cooling timescale of the envelope $\propto t_{\rm KH} \propto M_\bullet^{-2/3}$ that becomes longer than the fallback time for $M_\bullet \ll 10^6\ M_\odot$ (Equation (29)); thus, we would predict a flattening or turnover in the $t_{\rm rise}(M_\bullet)$ relationship found by V21 at the lowest $M_\bullet$ (or $M_{\rm gal}$). This also cautions against using rapid optical light-curve evolution as a property to identify TDEs by intermediate-mass black holes (IMBHs).

## 4. Conclusions

We have presented a model for TDE light curves, which starts from the assumption that circularization of the most tightly bound stellar debris is prompt (i.e., occurs on the fallback time of the most tightly bound debris), resulting in the creation of a quasi-spherical pressure-supported envelope surrounding the SMBH (Loeb & Ulmer 1997) with a characteristic size much larger than the circularization radius defined by the angular momentum of the original orbit (Coughlin & Begelman 2014). This assumption is motivated by recent hydrodynamical simulations that find prompt circularization and rising optical emission consistent with observed early phases of TDE flares, even for the most common "garden-variety" $\beta = 1$ disruptions (Steinberg & Stone 2022). Our model builds on earlier works starting with Loeb & Ulmer (1997) but focuses on predicting the long-term evolution of the envelope and its accretion rate onto the SMBH, under the influence of different sources/sinks of mass and energy, in a flexible, simple-to-implement, and simple-to-interpret format.

The proposed "cooling envelope" model accounts for a variety of TDE observations, including (1) large photosphere radii and correspondingly high optical luminosities; (2) optical light-curve decay, driven largely by passive cooling of the envelope, which roughly follows a power law $\nu L_\nu \propto t^{-3/2}$, coincidentally similar to the canonical $\propto t^{-5/3}$ rate of fallback decline; (3) potential at late times for a shallower or plateau-shaped light-curve decay, due to self-regulated energy input from SMBH accretion; (4) gradually rising effective temperature $T_{\rm eff} \propto t^{1/2}$ as the envelope contracts; and (5) delay in the peak of the SMBH accretion rate, and hence of thermal X-ray (for opportunely oriented viewers) or jetted emissions, relative to the time of optical peak by up to several hundred days. This delay is notably driven by envelope cooling (either acting in isolation or temporarily offset by SMBH accretion heating), rather than requiring a delay in the circularization process.

Our model does not itself account for the luminous X-ray emission observed at early times in some TDEs (e.g., Liu et al. 2022). However, recent numerical simulations show how soft X-ray emission may accompany the early phases of envelope formation (e.g., Bu et al. 2022; Steinberg & Stone 2022), before the establishment of a massive envelope and a large photosphere radius. Some of our models predict rapid X-ray brightening several months or years after the disruption, due to runaway accretion of the remaining envelope onto the SMBH, which could be compatible with X-ray observations of TDEs such as OGLE16aaa (which brightened by an order of magnitude in just 1 week; Kajava et al. 2020); however, the presence of this late abrupt $L_{\rm X}$ rise in our model is sensitive to the assumed envelope density profile (Figure 4). Some X-ray-selected TDEs also exhibit weak optical emission at early times (e.g., Sazonov et al. 2021), which in our scenario could be explained by a particularly short envelope cooling timescale, $t_{\rm KH} \propto m_\star^{13/15} M_\bullet^{-2/3}$, requiring a high-mass SMBH or low-mass disrupted star (Equation (28)). The volumetric rate of X-ray-selected TDEs appears to be significantly lower than the optically selected TDE rate (e.g., Stone et al. 2020; Sazonov et al. 2021), consistent with rapid-cooling envelopes being a modest fraction of the total TDE population.

An $\sim$Eddington-limited hydrostatic envelope scenario appears broadly consistent with correlations between TDE light-curve properties and host galaxy (proxy SMBH) mass (van Velzen et al. 2021a). On the other hand, the model is challenged to explain the observed positive correlation between proxy SMBH mass and optical decay time assuming that the latter tracks the Kelvin–Helmholtz time $t_{\rm KH,0} \propto M_\bullet^{-7/6}$ (Equation (28)); however, the shortness of $t_{\rm KH}$ relative to the fallback time $t_{\rm fb} \propto M_\bullet^{1/2}$ (Equation (29)) suggests that the light-curve shape near peak will be sensitive to the envelope assembly process and early-time fallback heating (Equation (30)), possibly mixing some $t_{\rm fb}$ dependence into

the decay time. Our model predicts a minimum evolution time for TDE optical light curves set by the cooling time of the envelope, which—contrary to the fallback timescale—grows toward smaller black hole masses. This would have implications for searching for IMBHs via optical TDE flares.

The end of our calculation, and thus of the most optically luminous phase, is defined by when the envelope contracts to the circularization radius, after which point rotational effects dominate and the disk structure should better resemble the pure $\alpha$-disk models originally envisioned (e.g., Rees 1988; Lodato & Rossi 2011). The properties of the remaining envelope at this transition may then define the initial conditions for a viscous disk evolution phase (e.g., Shen & Matzner 2014), which can power longer-lasting UV/X-ray emission (e.g., Auchettl et al. 2017; van Velzen et al. 2019; Jonker et al. 2020). The timescale of this transition depends on whether the envelope contraction is limited by radiative cooling or accretion and whether SMBH feedback slows the latter, but in general it can roughly be written as

$$t_{\rm life} = \min\left[t_{\rm disk}, \max[t^{\star}_{\rm acc}, t^{\bullet}_{\rm acc}]\right], \quad (43)$$

where $t_{\rm disk}$, $t^{\star}_{\rm acc}$, $t^{\bullet}_{\rm acc}$ are given in Equations (33), (34), and (38), respectively.

The prediction of a cooling-induced time delay of several months or longer between the peak of the optical light curve and the SMBH accretion rate may also bear on other puzzling TDE observations. One of these is the discovery of late-time radio flares or rebrightenings (e.g., Horesh et al. 2021a, 2021b; Cendes et al. 2022; Perlman et al. 2022; Sfaradi et al. 2022), which may indicate the delayed ejection of mildly relativistic material from the immediate viscinity of the SMBH several months to years after the optical peak. We speculate that these could arise from jets or winds from the inner accretion disk that suddenly become more powerful as the SMBH accretion rate rises rapidly near the termination of the envelope cooling −contraction phase. Shocks driven by such outflows into the surrounding wind/envelope material could in principle accelerate relativistic ions, generating a source of high-energy gamma-rays and neutrinos (Lunardini & Winter 2017; Senno et al. 2017; Guépin et al. 2018; Fang et al. 2020; Murase et al. 2020), perhaps explaining the significant observed delay between the high-energy neutrino detections from a growing sample of TDE and the optical light-curve maximum (van Velzen et al. 2021b; Stein et al. 2021; Reusch et al. 2022).

Although our model is constructed to allow for the effects of winds or outflows from the envelope on its evolution (the sink terms $\dot{M}_w$, $\dot{E}_w$ in Equations (13) and (14)), we have neglected this possibility for simplicity in this work. Strong outflows could occur from the envelope if energy is deposited below its surface at a highly super-Eddington rate (Quataert et al. 2016). We speculate that this may occur at two phases in the TDE: (1) at early times, when the envelope is being assembled and $R_{\rm acc} \lesssim R_v$ is small and hence $\dot{E}_{\rm fb} \gg L_{\rm Edd}$ is possible (Equation (30)); and (2) at late times as $R_v \rightarrow R_{\rm acc}$ and the SMBH accretion rate is quickly rising to high values, on a timescale faster than the envelope can radiate the received energy.

I am grateful to Elad Steinberg and Nicholas Stone for helpful comments and for sharing an early draft of their manuscript, which imparted momentum to this work. I also benefited from discussions with Sjoert van Velzen. I thank the anonymous referee for insightful comments. This work was supported in part by the NSF (grant No. AST-2009255). The Flatiron Institute is supported by the Simons Foundation.

## ORCID iDs

Brian D. Metzger https://orcid.org/0000-0002-4670-7509

## References

Alexander, K. D., van Velzen, S., Horesh, A., & Zauderer, B. A. 2020, SSRv, 216, 81
Alexander, K. D., Wieringa, M. H., Berger, E., Saxton, R. D., & Komossa, S. 2017, ApJ, 837, 153
Andalman, Z. L., Liska, M. T. P., Tchekhovskoy, A., Coughlin, E. R., & Stone, N. 2022, MNRAS, 510, 1627
Arcavi, I., Gal-Yam, A., Sullivan, M., et al. 2014, ApJ, 793, 38
Auchettl, K., Guillochon, J., & Ramirez-Ruiz, E. 2017, ApJ, 838, 149
Blagorodnova, N., Gezari, S., Hung, T., et al. 2017, ApJ, 844, 46
Blandford, R. D., & Begelman, M. C. 1999, MNRAS, 303, L1
Bloom, J. S., Giannios, D., Metzger, B. D., et al. 2011, Sci, 333, 203
Bonnerot, C., & Lu, W. 2020, MNRAS, 495, 1374
Bonnerot, C., & Lu, W. 2022, MNRAS, 511, 2147
Bonnerot, C., Rossi, E. M., & Lodato, G. 2016a, MNRAS, 458, 3324
Bonnerot, C., Rossi, E. M., & Lodato, G. 2017, MNRAS, 464, 2816
Bonnerot, C., Rossi, E. M., Lodato, G., & Price, D. J. 2016b, MNRAS, 455, 2253
Bonnerot, C., & Stone, N. C. 2021, SSRv, 217, 16
Bu, D.-F., Qiao, E., Yang, X.-H., & Liu, J. 2022, MNRAS, in press
Burrows, D. N., Kennea, J. A., Ghisellini, G., et al. 2011, Natur, 476, 421
Cannizzo, J. K., Lee, H. M., & Goodman, J. 1990, ApJ, 351, 38
Cao, R., Liu, F. K., Zhou, Z. Q., Komossa, S., & Ho, L. C. 2018, MNRAS, 480, 2929
Cendes, Y., Berger, E., Alexander, K., et al. 2022, arXiv:2206.14297
Cenko, S. B., Krimm, H. A., Horesh, A., et al. 2012, ApJ, 753, 77
Coughlin, E. R., & Begelman, M. C. 2014, ApJ, 781, 82
Coughlin, E. R., Nixon, C., Begelman, M. C., & Armitage, P. J. 2016, MNRAS, 459, 3089
Coughlin, E. R., & Nixon, C. J. 2022, ApJ, 926, 47
Dai, L., McKinney, J. C., & Miller, M. C. 2015, ApJL, 812, L39
Dai, L., McKinney, J. C., Roth, N., Ramirez-Ruiz, E., & Miller, M. C. 2018, ApJL, 859, L20
Evans, C. R., & Kochanek, C. S. 1989, ApJL, 346, L13
Fang, K., Metzger, B. D., Vurm, I., Aydi, E., & Chomiuk, L. 2020, ApJ, 904, 4
Generozov, A., Mimica, P., Metzger, B. D., et al. 2017, MNRAS, 464, 2481
Gezari, S. 2021, ARA&A, 59, 21
Gezari, S., Cenko, S. B., & Arcavi, I. 2017, ApJL, 851, L47
Gezari, S., Martin, D. C., Milliard, B., et al. 2006, ApJL, 653, L25
Giannios, D., & Metzger, B. D. 2011, MNRAS, 416, 2102
Guépin, C., Kotera, K., Barausse, E., Fang, K., & Murase, K. 2018, A&A, 616, A179
Guillochon, J., & Ramirez-Ruiz, E. 2013, ApJ, 767, 25
Guillochon, J., & Ramirez-Ruiz, E. 2015, ApJ, 809, 166
Hayasaki, K., Stone, N., & Loeb, A. 2013, MNRAS, 434, 909
Hayasaki, K., Stone, N., & Loeb, A. 2016, MNRAS, 461, 3760
Hills, J. G. 1975, Natur, 254, 295
Holoien, T. W. S., Kochanek, C. S., Prieto, J. L., et al. 2016, MNRAS, 463, 3813
Holoien, T. W.-S., Prieto, J. L., Bersier, D., et al. 2014, MNRAS, 445, 3263
Horesh, A., Cenko, S. B., & Arcavi, I. 2021a, NatAs, 5, 491
Horesh, A., Sfaradi, I., Fender, R., et al. 2021b, ApJL, 920, L5
Hung, T., Gezari, S., Blagorodnova, N., et al. 2017, ApJ, 842, 29
Jonker, P. G., Stone, N. C., Generozov, A., van Velzen, S., & Metzger, B. 2020, ApJ, 889, 166
Kajava, J. J. E., Giustini, M., Saxton, R. D., & Miniutti, G. 2020, A&A, 639, A100
Kara, E., Dai, L., Reynolds, C. S., & Kallman, T. 2018, MNRAS, 474, 3593
Leloudas, G., Fraser, M., Stone, N. C., et al. 2016, NatAs, 1, 0002
Liu, F. K., Cao, C. Y., Abramowicz, M. A., et al. 2021, ApJ, 908, 179
Liu, X.-L., Dou, L.-M., Chen, J.-H., & Shen, R.-F. 2022, ApJ, 925, 67
Lodato, G., & Rossi, E. M. 2011, MNRAS, 410, 359
Loeb, A., & Ulmer, A. 1997, ApJ, 489, 573
Lu, W., & Bonnerot, C. 2020, MNRAS, 492, 686
Lunardini, C., & Winter, W. 2017, PhRvD, 95, 123001
Magorrian, J., Tremaine, S., Richstone, D., et al. 1998, AJ, 115, 2285

Matsumoto, T., & Piran, T. 2021, MNRAS, 502, 3385
Metzger, B. D., & Stone, N. C. 2016, MNRAS, 461, 948
Miller, J. M., Kaastra, J. S., Miller, M. C., et al. 2015, Natur, 526, 542
Miller, M. C. 2015, ApJ, 805, 83
Murase, K., Kimura, S. S., Zhang, B. T., Oikonomou, F., & Petropoulou, M. 2020, ApJ, 902, 108
Patra, K. C., Lu, W., Brink, T. G., et al. 2022, MNRAS, 515, 138
Perlman, E. S., Meyer, E. T., Wang, Q. D., et al. 2022, ApJ, 925, 143
Phinney, E. S. 1989, in IAU Symp. 136, The Center of the Galaxy, ed. M. Morris (Dordrecht: Kluwer Academic Publishers), 543
Piran, T., Svirski, G., Krolik, J., Cheng, R. M., & Shiokawa, H. 2015, ApJ, 806, 164
Quataert, E., Fernández, R., Kasen, D., Klion, H., & Paxton, B. 2016, MNRAS, 458, 1214
Rees, M. J. 1988, Natur, 333, 523
Reusch, S., Stein, R., Kowalski, M., et al. 2022, PhRvL, 128, 221101
Roth, N., Kasen, D., Guillochon, J., & Ramirez-Ruiz, E. 2016, ApJ, 827, 3
Ryu, T., Krolik, J., & Piran, T. 2021, ApJ, 920, 130
Sadowski, A., & Narayan, R. 2016, MNRAS, 456, 3929
Sadowski, A., Tejeda, E., Gafton, E., Rosswog, S., & Abarca, D. 2016, MNRAS, 458, 4250
Sazonov, S., Gilfanov, M., Medvedev, P., et al. 2021, MNRAS, 508, 3820
Senno, N., Murase, K., & Mészáros, P. 2017, ApJ, 838, 3
Sfaradi, I., Horesh, A., Fender, R., et al. 2022, ApJ, 933, 176
Shakura, N. I., & Sunyaev, R. A. 1973, A&A, 24, 337
Shen, R.-F., & Matzner, C. D. 2014, ApJ, 784, 87
Shiokawa, H., Krolik, J. H., Cheng, R. M., Piran, T., & Noble, S. C. 2015, ApJ, 804, 85
Stein, R., Velzen, S. v., Kowalski, M., et al. 2021, NatAs, 5, 510
Steinberg, E., Coughlin, E. R., Stone, N. C., & Metzger, B. D. 2019, MNRAS, 485, L146
Steinberg, E., & Stone, N. C. 2022, arXiv:2206.10641
Stern, D., van Dokkum, P. G., Nugent, P., et al. 2004, ApJ, 612, 690
Stone, N., Sari, R., & Loeb, A. 2013, MNRAS, 435, 1809
Stone, N. C., Vasiliev, E., Kesden, M., et al. 2020, SSRv, 216, 35
Strubbe, L. E., & Quataert, E. 2009, MNRAS, 400, 2070
Tchekhovskoy, A., Metzger, B. D., Giannios, D., & Kelley, L. Z. 2014, MNRAS, 437, 2744
van Velzen, S., Farrar, G. R., Gezari, S., et al. 2011, ApJ, 741, 73
van Velzen, S., Gezari, S., Hammerstein, E., et al. 2021a, ApJ, 908, 4
van Velzen, S., Stein, R., Gilfanov, M., et al. 2021b, arXiv:2111.09391
van Velzen, S., Stone, N. C., Metzger, B. D., et al. 2019, ApJ, 878, 82
Wevers, T., Pasham, D. R., van Velzen, S., et al. 2019, MNRAS, 488, 4816
Yao, Y., Lu, W., Guolo, M., et al. 2022, arXiv:2206.12713